

Article

Electron Microscopy Evidence of Zn Bioauthigenic Sulfides Formation in Polluted Organic Matter-Rich Sediments from the Chicamocha River (Boyacá-Colombia)

Claudia Patricia Quevedo ¹, Juan Jiménez-Millán ^{2,*}, Gabriel Ricardo Cifuentes ³ and Rosario Jiménez-Espinosa ² 

¹ Grupo de Investigación Gestión Ambiental, Facultad de Ciencias e Ingeniería, Universidad de Boyacá, Campus Tunja, Tunja 15003, Colombia; patriciaquevedo@uniboyaca.edu.co

² Departamento de Geología y CECTEMA, Universidad de Jaén, Campus Las Lagunillas, 23071 Jaén, Spain; respino@ujaen.es

³ Grupo de Investigación Gestión de Recursos Hídricos, Facultad de Ciencias e Ingeniería, Universidad de Boyacá, Tunja 15003, Colombia; grcifuentes@uniboyaca.edu.co

* Correspondence: jmllan@ujaen.es

Received: 8 July 2020; Accepted: 28 July 2020; Published: 29 July 2020



Abstract: Electron microscopy and sediment geochemical data from a river basin (the upper Chicamocha river basin, UCRB, Boyacá province, Colombia) affected by anthropogenic activities (wastewater discharges, smelting and agricultural activities) showed the existence of heterogeneously distributed Zn particles in the sediments and sediments with Zn contents above the regional background (42 mg/kg). The objective of this study was to evidence the ZnS sedimentary neoformation in organic matter rich sediments deposited in anthropogenic reservoirs to reveal the processes involved in the sedimentary uptake of Zn from potential pollution sources. The highest Zn concentrations are found in clay minerals and organic matter-rich sediments (up to 427 mg/kg) deposited in slow-flowing reaches of the river associated to La Playa dam. Quartz-rich sediments poor in organic matter deposited in fast flowing segments of the river show very low Zn contents (1–12 mg/kg). Electron microscopy images showed ZnS nanoparticles forming cell-shaped aggregates suggesting that sulfate-reducing microorganisms acted as templates for the partial binding of Zn and for the nucleation and growth of zinc sulfide minerals. A good correlation of Zn with total organic carbon ($r = 0.936$) and the low potential redox of these sediments (-233 mV) suggest that organic matter was able to maintain oxygen depleted conditions appropriate to the Zn accumulation in the sediments. Our results demonstrate that potentially toxic Zn, originating from anthropic activities, was partially immobilized in organic matter-rich sediments through the precipitation of sulfides.

Keywords: ZnS nanoparticles; cell-shaped aggregates; Zn pollution; organic matter-rich sediments; microbial sulfate-reducing activity

1. Introduction

Pollution by heavy metals is of particular concern for humans because of their detrimental health effects on people in excessive quantities. Contaminated geomaterials in areas heavily utilized by people, including extensively used recreational zones in towns [1] or agricultural fields [2,3], can create potential risk of metal exposure to humans. Alluvial sediments in river basins can accumulate or release heavy metals depending on flow regime and flooding [4]. The presence of dams regulate the surface water outflow in river basins and causes slow-flowing sites and flooding. The accumulation of clays and organic matter is favored behind these dams, promoting in many cases binding of metals.

Zn is present in many polluted sediments due to anthropogenic activities. Zn is an essential microelement, and it is toxic only in high concentrations [5]. Due to its toxicity and irreversible consequences, this metal has been included in the list of priority control pollutants of the US Environmental Protection Agency (US EPA, Washington, DC, USA) [6,7]. The estimated global average content of Zn in soil and surficial sediments is 64 mg/kg [8]; its concentration is mainly controlled by the texture, organic matter content and pH. Industrial activities, such as smelting, and agricultural practices, such as wastewater irrigation or intensive application of pesticides and fertilizers, are potential sources of this metal in sediments [3,9].

Smelting of metals is one of the major anthropogenic sources of Zn pollution in the environment, e.g., [1,7], causing sediment, water and soil contamination with high metal concentrations caused by the atmospheric deposition of smelter emissions, frequently even at concentrations that require some form of remediation. The frequent use of Zn-bearing phosphate fertilizers, pesticides, herbicides and fungicides can also have an important effect on the concentration of this metal in sediments [3].

Zn mobility, bioavailability, and toxicity, which are key factors in assessing risks to ecosystems and human health, depend strongly on its specific chemical forms and reactivity [10,11]. Zn entrapment within the crystal structure of certain minerals reduces its mobility and availability. Although the speciation of Zn is complex, oxy-hydroxy substances have been found to control sorption/desorption behavior [12,13], while reduced sulfide species, either HS^- or $\text{S}^=$ in solution or sulfur-containing functional groups in organic matter, have a very strong affinity for Zn. In reducing organic matter environments, sulfides can react with divalent metals in solution, such as Zn, and are able to remove this metal as insoluble sulfide [14]. Microbes can control metal concentrations in wetland remediation systems through the formation of low-temperature ZnS deposits [15]. The low solubility of the Zn-bearing sulfide phases favors Zn removal, maintaining its concentration in waters below the acceptable levels while the anoxic conditions prevail [16].

Constructed wetlands containing sediments rich in organic matter and saline waters provide appropriate environments for aqueous reduction processes, frequently associated to reducing microorganism activity, that promote the production of sulfide, which can form insoluble sulfides of divalent metals [17]. The immobilization of toxic metals by precipitation reactions in the sediments of these environments can significantly contribute to remediate the presence of pollutants by natural attenuation processes. High-resolution electron microscopy studies are one of the best tools to determine the presence of these minerals, their size, shape, chemical composition, and distribution in organic matrix. The use of these techniques provides significant data to elucidate some of the factors controlling the formation of the insoluble phases, such as the microbial–mineral interactions or the changes in aqueous and sediment chemistry [18].

The Upper Chicamocha River Basin (UCRB) (Boyacá province, Colombia) is characterized by the presence of dams that regulate the westward surface runoff water and produce artificial wetlands. The La Playa dam is one of most representative wetlands [19] used for different water supplies, such as livestock, agriculture, tourism and industry. Its impoundment receives anthropogenic inputs from farm activities (using fertilizers and pesticides) and wastewaters (mainly urban sewage) [20] that have produced high-salinity waters, intense eutrophication and organic matter-rich sediments. These inputs could also produce heavy metal accumulation in water and sediments. Moreover, the La Playa dam is located in Tuta, less than 3 km east of an important smelter that produce smelting slags with high Zn contents [21]. Despite the existence of these important threats for water and sediment quality, previous studies on the heavy metal contamination extent have been scarce, especially for Zn [20,22]. The absence of relevant data and lack of knowledge of the factors controlling the behavior of Zn in the sediments of the basin prompted this study as part of the monitoring program promoted by the Boyacá Regional Agency for the Environment (Corpoboyacá, Tunja, Colombia). This paper reports mineralogical and geochemical data to identify accumulation areas and potential sources of Zn (together with Cu, Pb, Cr and Ni) at 20 sites within the UCRB alluvial system, covering a region of approximately 100 km².

This study was especially focused on the use of high resolution microscopy techniques (field emission scanning electron microscopy, FESEM, and high-resolution transmission electron microscopy HRTEM), coupled to energy dispersive X-ray spectrometry (EDX) to evidence the ZnS sedimentary neoformation in organic matter rich sediments deposited in anthropogenic reservoirs to reveal the processes involved in the sedimentary uptake of Zn from potential pollution sources in the UCRB area.

2. Background Context

The UCRB is located in the high mountains of the equatorial Andes of Colombia in the Boyacá department (Figure 1). The landscape is characterized by plains of lacustrine and fluvio-lacustrine origin, with average heights over 2500 m, surrounded by elevated massifs and plateaus (2650–2800 m), including the Tunja Plateau [23]. The area of the UCRB is around 214,000 ha, with a length of 62.46 km and an average slope of 0.12% [24]. The Chicamocha river is formed by the confluence of the Tuta and Jordán rivers with a length of 227 km flowing to the Caribbean Sea.

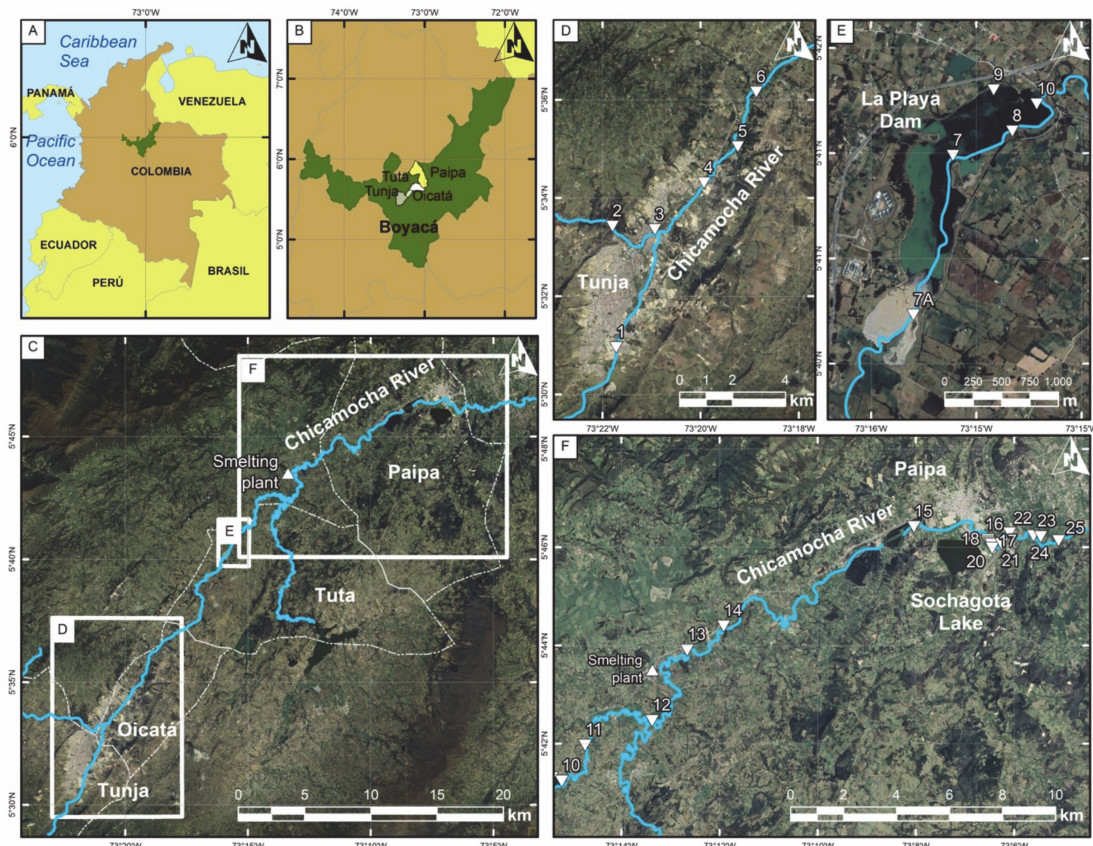


Figure 1. Geographical setting of the study area and sampling location. (A) Global context of the area; (B) Regional map; (C) Studied sector of the Chicamocha River between Tunja and Paipa, Boyacá Province; (D–F) Location of the sampling points 1 to 25.

Regarding the climate of the UCRB, annual rainfall ranges from 650–800 mm in the southwestern area to 900–1200 mm in the northwestern area. The highest precipitations occur during April–May and October–November. The average annual temperature is around 13.1 °C. March and November are the warmest months. Prevailing wind directions are from east and north.

The Chicamocha River Basin is characterized by the presence of Paleozoic to Quaternary sedimentary and volcanic rocks. Sedimentary rocks are predominantly siliceous (conglomerates, sands, shales and clays). The Paipa sector is characterized by the presence of one of the main geothermal areas in the Colombian territory. At the northwestern sector of the UCRB the products of the Paipa

volcano crops out, which is an eroded explosive volcanic building formed by acid pyroclastic deposits (alkaline rhyolites and trachyandesites) of the Pliocene–Pleistocene age [24].

The most important anthropogenic modification of the UCRB is La Playa dam. The La Playa dam is located at the Tuta area in the upper sector of the URCB (Figure 1). This reservoir supplies water for livestock and agricultural activities and receives wastewaters (urban sewage) from Tunja, Oicatá, Combita and Tuta, together with runoff waters of the surrounding farming activities, generating high organic and nutrient load [25]. All of these inputs produce an intense eutrophication with a strong proliferation of *Eichhornia crassipes* and colonies of small algae, such as *Trachelomonas* and *C. microporum* [19]. Nearby La Playa dam, in the Tunja-Paipa road (km 27), is a manufacturing facility belonging to one of the world's largest steel producers. This facility produces recycled carbon steels causing the emission of slags with high Zn contents [21]. The presence of other heavy metals has not been investigated.

3. Materials and Methods

3.1. Materials

Sediments of the river were sampled from a 20 points network through the UCRB, including proper alluvial deposits and sediments from La Playa dam (Figure 1D–F). A standard stainless Shelby tube was used for sampling, and cores down to a depth of 50 cm were obtained. The physico-chemical parameters of sediments (redox potential, pH and electrical conductivity) were determined in situ with a Hanna Instruments multiparameter for soils and sediments (HI98168, Hanna Instruments (S) Pte Ltd., Singapore). The sediment samples were dried in oven at 40 °C and prepared for further treatments. Sediment fragments were picked every 10 cm in the cores for the electron microscopy studies. For the X-ray diffraction (XRD), X-ray fluorescence (XRF) and Inductively Coupled Plasma-Mass spectrometry (ICP-MS) studies, each core was homogenized to yield a single sample. Water samples were also taken from the same 20 sampling points (Figure 1). At each site, water samples were collected in several (15, 50 and 150 mL) clean high-density polyethylene bottles (HDPE), rinsed several times with groundwater to be sampled. One of the bottles (15 mL) containing sample was acidified to pH < 2.0 with nitric acid (HNO₃), ACS reagent and a purity of 70 %, to stabilize trace metals. The filling of the bottles was performed using sterile syringes and filtered by a 0.45-μm filter pore size then acidified. The samples were stored in ice boxes, brought to laboratory and stored at 4 °C for ICP-MS analysis.

3.2. Mineralogical and Geochemical Analysis

The XRD data were obtained of oriented aggregates from the homogenized whole sample and from the <2 μm fraction of the same sample separated by centrifugation, after washing with ultrapure water to remove salts. Oriented aggregates were prepared by settling a dispersion in a glass holder. Furthermore, ethylene glycol treatment was carried out to assist in the identification of expandable minerals (smectite, interstratified layers, etc.). The diffraction patterns were obtained in a Panalytical X'Pert Pro diffractometer (CuKα radiation, 45 kV, 40 mA, Panalytical, Eindhoven, The Netherlands) equipped with an X'Celerator solid-state linear detector, using a step increment of 0.008° 2θ and a counting time of 10 s/step (Centro de Instrumentación Científico-Técnica of the Universidad de Jaén, Spain). A sweep between 3° and 62° 2θ was done on the dry samples, while for the glycolated samples the sweep was done between 2° and 30° 2θ in order to confirm the identification of expandable minerals. Deconvolution routines included in the HighScore software were applied.

Textural and chemical observations in a field emission scanning electron microscope (FESEM, Merlin Carl Zeiss, Carl Zeiss, Oberkochen, Germany) were made on polished sections using back-scattered electrons (BSE) in atomic number contrast mode, and on sediment fragments in secondary electron mode (SE). Chemical composition of minerals was obtained using an energy dispersive X-ray spectrometry (EDX) coupled to the electron microscope. The FESEM study was

carried out with a Merlin Carl Zeiss (Carl Zeiss, Oberkochen, Germany) equipment with an Oxford Inca EDX system in the Centro de Instrumentación Científico-Técnica of the Universidad de Jaén.

For the textural and chemical characterization at the nanometer scale, selected samples according to XRD analysis and FESEM observations were prepared for high resolution transmission electron microscopy (HRTEM) study. Samples were prepared using Au and Cu grid surface coated in a perforated formvar resin from a dispersion of finely ground sample particles, in alcohol or distilled water. The monomineralic character of each grain is proven by its electron diffraction pattern, checking the existence of a single network and, therefore, a single crystalline phase. The sections were then fixed on an Au or Cu grid for TEM analysis. The TEM data were obtained using two electron microscopes at the Centro de Instrumentación Científica (C.I.C.) of the Universidad de Granada (Granada, Spain): the HAADF FEI TITAN G2 microscope, operated at 300 kV, and the Philips CM20 microscope, operated at 200 kV. Qualitative analyses (AEM) of particles were obtained with an EDX microanalysis system in the Philips CM20.

Whole-sediment analyses of the major and trace elements of selected samples were carried out using XRF in a Philips Magix Pro (PW-2440) spectrometer. Every sample was finely powdered in a mill and then pressed into a pellet using wax, producing a dense and homogenous sample to enhance the analytical performance of trace elements [26]. Glass beads with lithium tetraborate were also employed for the major elements analyses to minimize the preferential orientation of phyllosilicates. The detection limit was 0.01 wt.% for major elements and from 1 to 5 mg/kg for trace elements. An empirical calibration was performed with an array of more than 25 international geostandards, including a wide range of silica-containing common rocks (Pro-trace reference materials, Panalytical). Residual matrix effects are adjusted taking into account a rough analysis of the main elements and using variable influence coefficients (alpha) obtained by fundamental parameters. Loss on ignition (LOI) was determined using 0.5 g of powdered sample, first dried at 110 °C and then heated at 1000 °C for one hour. Trace elements were also analyzed using a NexION 300D inductively coupled plasma-mass spectrometer (ICP-MS) (PerkinElmer Inc., Shelton, CT, USA). ICP-MS analyses were performed following sample digestion with HNO₃ + HF. Sample powders (0.1 g) were attacked in a teflon-lined vessel at high temperature and pressure, and then evaporated to dryness. Subsequently, residues were dissolved in 100 mL of 4% vol. HNO₃. ICP-MS analyses quantification was made with certified standards (MAG-1, UB-N, AGV-N, DR-N, GS-N, GA, GH and BR-N). Waters were also analyzed by ICP-MS. Detection limit for all the trace elements analyzed was below 1 µg/kg. Three replicates were performed for each sample. Standard deviation was always below 5%. Both techniques, XRF and ICP-MS, were carried out at the Centro de Instrumentación Científica, CIC, Universidad de Granada, Granada, Spain.

The total organic carbon (TOC) was analyzed using a Shimadzu Total Organic Carbon Analyzer (TOC-V sch) from the Instituto de Recursos Naturales Agrobiología (IRNAS) from CSIC-Sevilla (Sevilla, Spain).

4. Results

4.1. XRD Results

XRD diffraction patterns reveal that the mineral assemblage of the alluvial sediments from the Chicamocha River is dominated by the presence of quartz and kaolinite. Some sediments from the southwestern and northeastern parts of the UCRB are enriched in quartz (Figure 2a). Kaolinite is the dominant phyllosilicate in all the studied samples with intense and sharp 7.2 and 3.6 Å peaks (Figure 2a). Mineral assemblage is contrastingly different in sediments from La Playa reservoir at the central part of the UCRB, where oriented aggregates of the <2 µm fraction have a broad peak of 10 to 13 Å (Figure 2b) due to the presence of smectite and illite-dioctahedral vermiculite mixed layers (I-DV) [27]. The presence of these minerals and the higher intensity of the kaolinite peaks indicate that the sediments from La Playa are enriched in clay minerals.

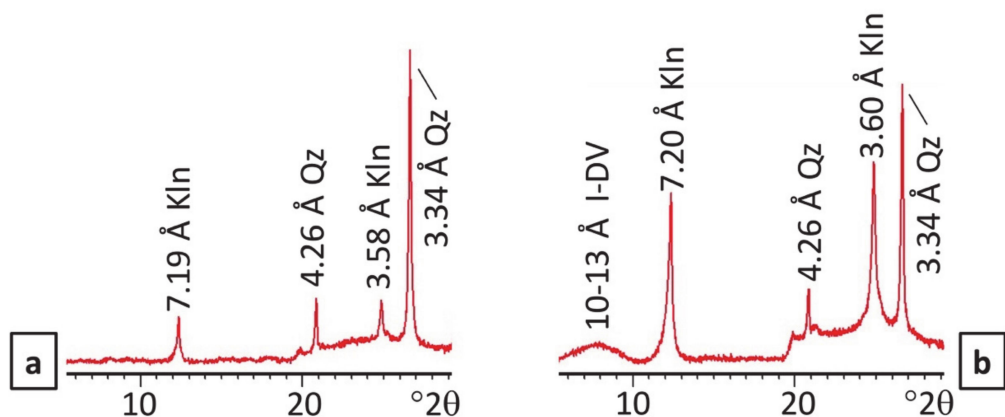


Figure 2. Representative diffractograms of oriented aggregates ($<2\mu\text{m}$ fraction) from sediments of the UCRB sediments. (a) Sediments from the northeastern part of the basin. (b) Sediments from the La Playa dam.

4.2. Electron Microscopy Results

SEM images of the sediments from the La Playa dam are characterized by alternating bands of microlaminated organic matter-rich layers and very fine-grain-sized clay-rich layers ($<2\mu\text{m}$) (Figure 3a). TEM-AEM study of the sediments from the La Playa dam confirmed the existence of three groups of clays: kaolinite, I-DV and smectite (Figure 3b).

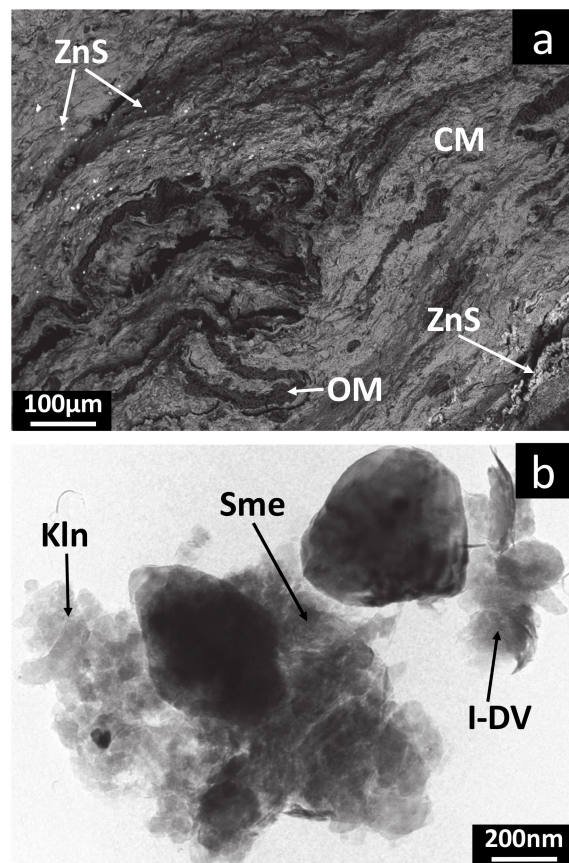


Figure 3. Cont.

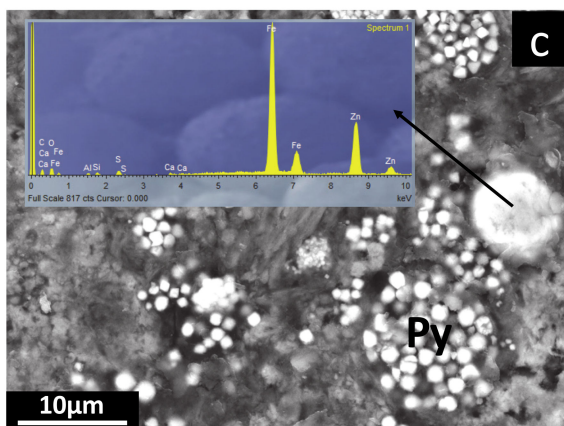


Figure 3. Electron Microscope images of the sediments from La Playa dam. (a) Back scattered electron image of alternating bands of microlaminated organic matter-rich layers (OM) and very fine-grain-sized clay-rich layers (CM). ZnS appears as dispersed small-sized particles and crusts. (b) Low magnification transmission electron microscope image of the sediments from La Playa dam showing the presence of pseudohexagonal crystals of kaolinite and very fine grain sized flakes of I-DV crystals and smectite. (c) Smelting particle containing Fe and Zn near pyrite framboids in organic matter-rich sediments. Kln: kaolinite. Sme: smectite. I-DV: illite-dioctahedral vermiculite mixed layers.

Quevedo et al. [27] indicated that the mineral assemblage in the sediments trapped in La Playa dam is characterized by the presence of Fe^{2+} -bearing smectite (up to 0.4 atoms per formula unit), pyrite microframboids and vivianite (iron phosphate), suggesting the existence of reduced conditions in the sediments. Small smelting particles containing Fe and Zn near pyrite framboids can also be observed (Figure 3c).

SEM and TEM imaging revealed the presence of ZnS aggregates associated to plant fragments (Figures 3a and 4a). Clumps of fine ZnS nanoparticles (50–100 nm) were observed forming aggregates with oval and spherical shape and size between 1 to 2 μm , closely resembling bacterial cell morphology (Figure 4b). Surfaces of the cell-shaped aggregates are heavily encrusted. Zn nanoparticles apparently not associated with cell-like morphologies were also observed in electron microscope images. HRTEM images (Figure 4c,d) shows that ZnS nanoparticles can occur scattered or attached to mineral surfaces. Several cell-shaped aggregates are apparently flattened probably as a consequence of the electron microscopy vacuum conditions or breaking down of the cells (Figure 4b,h). Grape-like clusters made up of multiple fragments of aggregated spheres (i.e., botryoidal habit) formed by coalescence or aggregation of microspheroids can also be observed (Figure 3a). SEM-EDX elemental mapping revealed that cell-shaped aggregates and extracellular precipitates contained Zn and S (Figure 4e–g); however, it was not possible to assign mineralogy at this scale because we could not obtain electron diffraction patterns even in the HRTEM. Although EDX analysis in FESEM confirmed that precipitates were mainly composed of zinc and sulfur, some of the ZnS particles have small contents of copper (Figure 4h,i). High concentrations of Si, O, Al, and K in silicate minerals of the sediments can explain the presence of these peaks in the EDX analyses (Figure 4h,j). P peak can be associated to the presence of vivianite crystals.

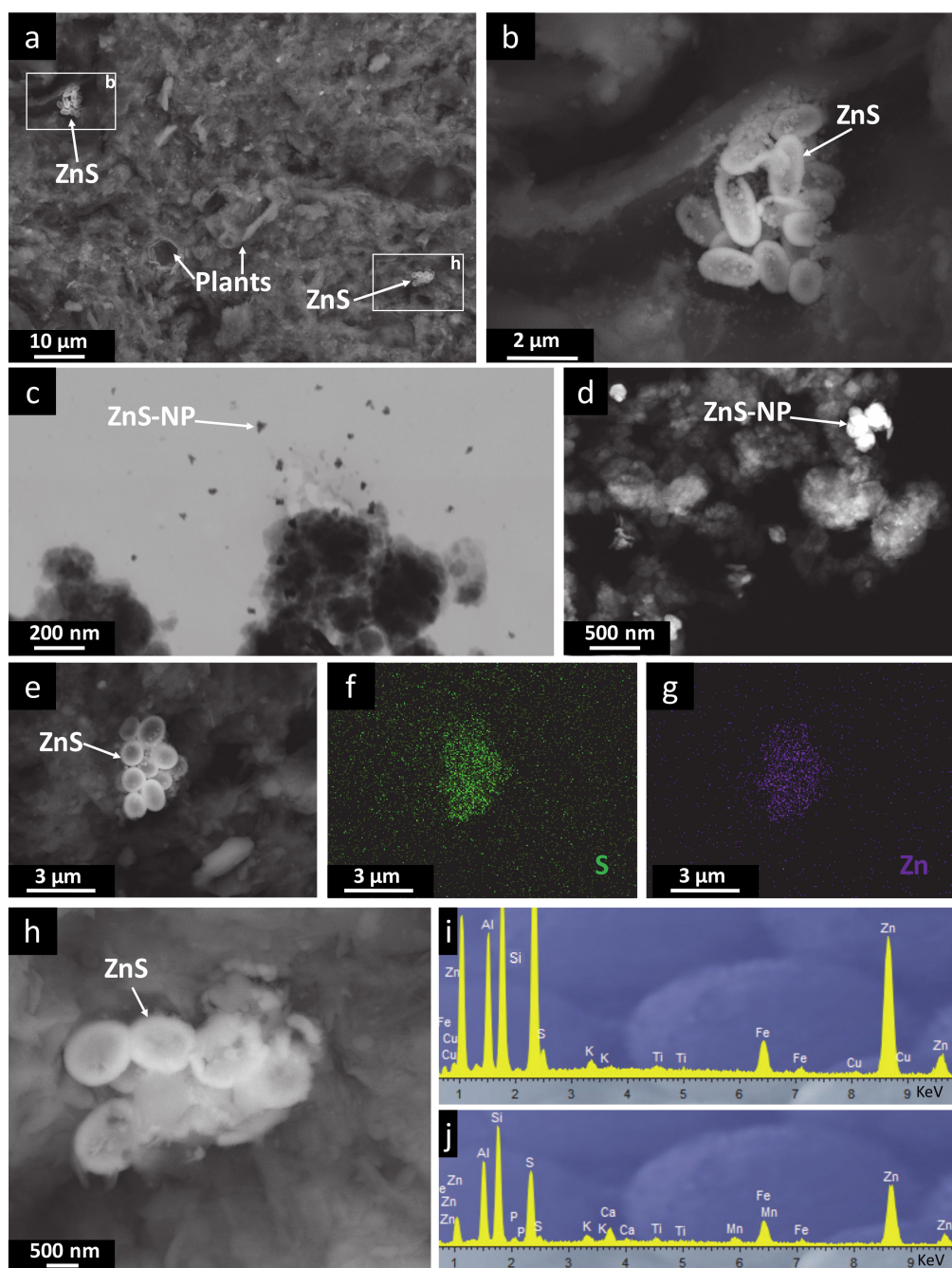


Figure 4. FESEM and HRTEM images of the ZnS-bearing sediments from La Playa dam. (a) FESEM image of ZnS aggregates associated to plant fragments. Squares indicate the location of (b,h); (b) ZnS nanoparticles forming aggregates which oval and spherical shape and size closely resemble bacterial cell morphology; (c,d) HRTEM images showing ZnS nanoparticles scattered or attached to mineral surfaces; (e) FESEM image of ZnS cell-shaped aggregate; (f) elemental map (EDX) of S (image f); (g) elemental map (EDX) of Zn (image f); (h) FESEM image of flattened cell-shaped aggregates due to cell collapse by cell lysis or EM sample preparation; (i,j) EDX spectra of ZnS cell-shaped aggregates.

4.3. Chemical Composition and Physicochemical Properties of the Sediments

The SiO_2 and Al_2O_3 contents of the sediments define two main group of samples. Clay-rich sediments from la Playa reservoir have lower SiO_2 contents (mean 61.24%) and higher Al_2O_3 contents (mean 17.17%) than quartz-rich sediments from the rest of segments of the UCRB (Table 1 and Table S1). The La Playa sediments are also characterized by the highest content in organic matter (TOC up to

13.84%), and LOI values (up to 15.43%). The quartz-rich sediments from the SW and NE part of the UCRB show the highest content in SiO₂ (up to 95.4%) and the lowest content in organic matter (TOC from 0.15% to 0.52%) and LOI values (0.72–1.55%). A significant variation on the P₂O₅ content of the sediments can also be observed, ranging from a mean value of 0.58% in the sediments from La Playa to 0.14% in the sediments from the northeastern segment of the UCRB.

Table 1. Major element sediment compositions determined by XRF and content in total organic carbon (TOC) (in weight percent). SD: Standard Deviation; Max: Maximum; Min: Minimum. Complete dataset is available in the Supplementary Materials (Table S1).

Values	SiO ₂	Al ₂ O ₃	FeO	MnO	MgO	CaO	Na ₂ O	K ₂ O	TiO ₂	P ₂ O ₅	LOI	TOC
SW segment. Upstream La Playa dam (<i>n</i> = 6)												
Mean	79.84	8.72	3.69	0.02	0.25	0.39	0.09	0.36	0.59	0.24	5.57	1.84
Median	81.18	7.60	3.07	0.02	0.25	0.33	0.10	0.35	0.57	0.32	5.70	1.90
SD	4.00	2.58	1.10	0.01	0.02	0.18	0.01	0.05	0.12	0.13	1.43	0.46
Max	84.01	13.32	5.40	0.04	0.27	0.61	0.11	0.46	0.80	0.33	7.48	2.49
Min	73.60	6.79	2.89	0.01	0.22	0.18	0.07	0.31	0.48	0.07	3.66	1.22
Central segment. La Playa reservoir (<i>n</i> = 4)												
Mean	61.24	17.17	4.05	0.01	0.14	0.39	0.06	1.12	0.42	0.58	14.37	10.72
Median	60.76	17.22	4.00	0.01	0.13	0.39	0.07	1.11	0.44	0.59	15.38	12.40
SD	1.44	0.92	0.26	0.00	0.02	0.23	0.04	0.20	0.07	0.04	2.61	4.49
Max	63.24	18.24	4.38	0.01	0.17	0.61	0.10	1.35	0.48	0.61	16.22	13.80
Min	60.18	15.99	3.81	0.01	0.12	0.18	0.02	0.91	0.31	0.51	10.51	4.29
NE segment. Downstream La Playa dam (<i>n</i> = 10)												
Mean	87.28	4.15	1.88	0.03	0.15	0.20	0.12	0.41	0.34	0.14	3.75	1.19
Median	89.60	2.16	1.39	0.01	0.12	0.16	0.10	0.29	0.25	0.09	2.03	0.68
SD	8.41	3.66	1.35	0.04	0.10	0.15	0.04	0.29	0.26	0.12	3.25	1.10
Max	96.25	11.57	5.01	0.13	0.41	0.55	0.20	1.23	0.87	0.36	10.83	3.61
Min	69.62	1.27	0.57	0.01	0.06	0.06	0.08	0.20	0.09	0.03	0.72	0.15
Unpolluted sediment (<i>n</i> = 15)												
Mean	91.74	5.66	2.46	0.02	0.17	0.25	0.12	0.36	0.42	0.16	4.00	1.28

Heavy metal concentrations in sediments from the UCRB vary depending on the sediment location. Sediments from La Playa reservoir contain comparatively high levels of heavy metals (Table 2 and Table S2) following a decreasing order as: Zn > Cu > Cr > Ni > Pb. On the other hand, lower mean values of these elements in the sediments from the NE and SW segments can be observed. Water composition of the sediment sampling sites (Table 3 and Table S3) is also characterized by higher heavy metals concentrations in samples from La Playa reservoir, especially for Zn (mean value 268 µg/L).

Table 2. Trace element sediment compositions determined by ICP-MS (for Cr, Ni, Cu and Pb) and XRF (for Zn) (in mg/kg). SD: Standard Deviation; Max: Maximum; Min: Minimum. Complete dataset is available in the Supplementary Materials (Table S2).

Sample	Cr	Ni	Cu	Zn	Pb
SW segment. Upstream La Playa dam (<i>n</i> = 6)					
Mean	62	58	76	96	20
Median	48	41	64	71	20
SD	38	39	35	83	10
Max	133	130	142	264	35
Min	28	22	47	43	5
Central segment. La Playa reservoir (<i>n</i> = 4)					
Mean	184	144	262	423	40
Median	184	138	204	415	38
SD	8	33	133	86	10
Max	192	190	459	534	54
Min	175	112	180	328	29
NE segment. Downstream La Playa dam (<i>n</i> = 10)					
Mean	30	22	34	43	10
Median	15	12	17	24	7
SD	45	26	35	53	8
Max	161	81	110	191	28
Min	5	5	6	5	5
Unpolluted sediment (<i>n</i> = 15)					
Mean	29	26	41	42	12

Table 3. Trace element water compositions at the sampling sites determined by ICP-MS (in $\mu\text{g/L}$). SD: Standard Deviation; Max: Maximum; Min: Minimum. Complete dataset and field water parameters are available in the Supplementary Materials (Table S3).

Sample	P	Cr	Ni	Cu	Zn	Pb
SW segment. Upstream La Playa dam (<i>n</i> = 6)						
Mean	419	1	4	8	43	1
Median	410	1	3	7	35	1
SD	246	0	1	2	20	0
Max	680	1	5	10	78	2
Min	30	0	2	6	28	0
Central segment. La Playa reservoir (<i>n</i> = 4)						
Mean	7280	3	7	23	268	4
Median	7098	4	7	23	249	4
SD	556	2	1	9	146	2
Max	8078	6	8	33	459	5
Min	6847	1	5	12	115	2
NE segment. Downstream La Playa dam (<i>n</i> = 10)						
Mean	221	0	2	4	27	1
Median	183	0	1	3	24	1
SD	172	0	1	3	14	1
Max	675	1	4	10	61	3
Min	14	0	1	1	14	0

The concentrations of Zn in the sediments from the UCRB exhibited large variability, ranged from 5 to 427 mg/kg (Table 2). The lowest concentrations (5–12 mg/kg) were found in the quartz-rich sands from the northern part of the basin. In the sediments rich in clay minerals and organic matter (TOC up to 13.84%) from the La Playa reservoir, Zn can be up to 427 mg/kg, i.e., more than 400 times the content in the quartz-rich sediments poor in organic matter. Zn is well correlated with TOC and LOI (Figure 5, Table 4) and with the other heavy metals and P_2O_5 .

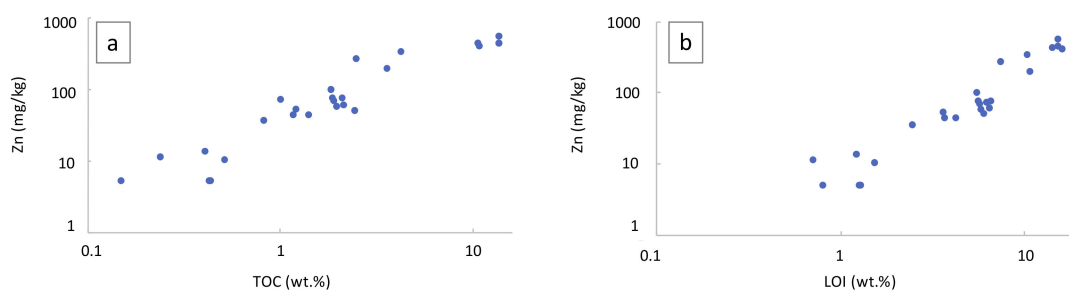


Figure 5. (a) Concentrations of Zn versus TOC in the UCRB sediments; (b) Concentrations of Zn versus LOI in the UCRB sediments.

Table 4. Pearson correlation matrix for heavy metals, TOC, LOI and P_2O_5 in sediment samples. Correlations are significant at the 0.01 level according to Student's t-test.

Variable	Cr	Ni	Cu	Zn	Pb	TOC	LOI	P_2O_5
Cr	1	0.960	0.854	0.942	0.919	0.828	0.932	0.871
Ni		1	0.848	0.899	0.898	0.732	0.857	0.855
Cu			1	0.935	0.792	0.860	0.851	0.816
Zn				1	0.888	0.942	0.936	0.883
Pb					1	0.942	0.936	0.883
TOC						1	0.922	0.832
LOI							1	0.751
P_2O_5								1

Table 5 and Table S4 show important differences in the physicochemical properties of the UCRB sediments and waters. La Playa sediments are characterized by lower redox potential (around -230 mV) and higher electrical conductivity ($2625\text{ }\mu\text{S/cm}$) than the rest of sediments.

Table 5. Physicochemical properties of the UCRB sediments. R.P.: Redox potential. E.C.: Electrical conductivity. Physicochemical properties of the waters are available in the Supplementary Materials (Table S4).

Segments of the UCRB	pH	R.P. (mV)	E.C. ($\mu\text{S/cm}$)
SW segment. Upstream La Playa dam ($n = 6$)	7.3	62	241
Central segment. La Playa reservoir ($n = 4$)	7.1	-233	2625
NE segment. Downstream La Playa dam ($n = 10$)	7.4	89	189

5. Discussion

5.1. Flow Regime and Flooding of the Chicamocha River and Sediment Conditions

The influence of flow regime and flooding of the Chicamocha river determined the formation of two main types of alluvial sediments in the basin. The river segment with slow-flowing conditions due to the construction of La Playa dam is characterized by the deposit of organic matter (TOC up to 16.22%, Table 1) and clay-rich sediments by periodic flooding. This reservoir receives input of untreated urban wastewaters and farming activities in the surrounding areas [27]. Domestic wastewater is considered one of the major sources of phosphate and nitrogen compounds in the natural environment, along with agricultural runoff [28]. Phosphate is a nutrient for algae that promotes eutrophication of water bodies. Eutrophication has many negative effects on aquatic ecosystems, such as proliferation of algae, degradation of water quality and oxygen depletion. The pollution of water by P in urban wastewater and agricultural runoff caused the intense eutrophication of the La Playa reservoir segment in the UCRB. The authigenic precipitation of Fe^{2+} -bearing sulfides, phosphates and smectites in the La Playa reservoir [27] reveals the existence of anoxic conditions (with measured redox potential around

–230mV) (Table 5) in the sediments rich in decaying organic matter with high microbiological activity caused by eutrophication.

In contrast, alluvial sediments deposited in fast-flowing sites, located both upstream and downstream of the La Playa dam, hardly contained organic matter (TOC frequently below 2.5%, Table 1), except for sample 14, situated in a local meander). In these cases, fast-flowing segments avoided the organic matter deposit and favored the water and sediment oxygenation (measured redox potential around 150mV).

5.2. Heavy Metal Distribution in Sediments and Pollution Sources

A decreasing order of Zn > Cu > Cr > Ni > Pb was observed in the mean values of the heavy metal contents in sediments from the La Playa slow- and fast-flowing segments located upstream and downstream of the La Playa. However, the heavy metal contents of the UCRB sediments vary depending on the location of the sediments, the mineral composition and the organic matter content (Tables 1 and 2).

There were significant differences between the Zn concentrations in different types of sediments from the UCRB. Zn contents in quartz-rich and organic matter-poor sediments (TOC contents below 2.5%) deposited in fast-flowing reaches of the Chicamocha river located upstream and downstream the La Playa dam are frequently below the corresponding values determined for some proposed unpolluted reference soils in Colombia (Table 2) [3] and clearly lower than crustal and average worldwide soils (around 70 mg/kg, [29]). Some sediments from these river segments richer in clay minerals and moderate TOC content (around 2.5%) have Zn concentrations similar to the crustal and average worldwide soils, although higher than average Zn contents in several regions (around 30–40 mg/kg [30,31]). According to these data, we considered the mean value of the quartz-rich with TOC contents below 2.5% deposited in fast-flowing reaches of the Chicamocha river located upstream and downstream the La Playa dam as a reference for the unpolluted sediments of the UCRB area (Tables 1 and 2).

On the other hand, the concentrations of Zn in the clay minerals and organic matter-rich sediments from the UCRB located in the slow-flowing reaches of the La Playa dam clearly exceeded the world normal averages (up to six times) and the mean level of Zn in these sediments was clearly higher than the corresponding value determined for the unpolluted reference sediment of the UCRB (Table 2). Although Colombia does not have a regulatory framework for concentrations of contaminants in sediments and soils [32,33], the Zn contents of the sediments from La Playa dam are above the threshold background values in European soils [34]. These Zn concentrations can be directly associated with an anthropogenic source.

Heavy metal accumulation in sediments and soils can be the result of different types of anthropic activities. Smelting, urban wastewater and agricultural activities can be considered as potential pollution sources that provided heavy metals to sediments of the UCRB. Smelting is one of the most significant sources of Zn pollution [35]. During smelting, Zn is usually released into the surrounding environment, e.g., [36,37], discharged with smelting gases which particles can accumulate in nearby soils and sediments leading to significant pollution [38,39]. The presence in the study area of a major manufacturing facility in the region, suggests this smelting site as one of the potential sources of pollution. According to Parra and Sánchez [21], this facility produced smelting slags representing a significant environmental hazard due to its high Zn contents (1728 mg/kg), but the presence of other metals was not reported. Slags are processed by grinding and milling producing additional emission of dust particles. The presence of small Fe-Zn particles in the sediments (Figure 3c) suggest that part of Zn was deposited in the sediments by atmospheric deposition of particles from the smelting plant. Zn-transport in solution or as particulate by runoff from this source is less probable because the smelting plant of the UCRB is located downstream the site that contain sediments with highest Zn-pollution (La Playa reservoir).

On the other hand, good correlations among P_2O_5 , heavy metals and organic matter contents (Table 4) suggest that the wastewater discharged by urban districts (e.g., Tunja, Figure 1) into the Chicamocha River, the use of wastewater irrigation and the frequent use of heavy metals-bearing products (fertilizers, pesticides, etc.) in the agricultural activities upstream the La Playa dam can also be considered as other potential sources for the concentration of heavy metals in the sediments deposited by periodic flooding in this area. In Colombia, the intensive use of fertilizers and pesticides was identified as an important source of pollutants in soils from river basin systems [3,32,40]. Flooding conditions could provide adequate conditions for the concentration of Zn and other heavy metals in the organic matter-rich sediments deposited by repeated inundation events [4].

5.3. The ZnS Formation

Good correlation of Zn with TOC ($r = 0.942$) and LOI ($r = 0.936$) (Table 4) suggest that clay minerals and organic matter are related with the accumulation of this metal in the sediments of the La Playa reservoir in the UCRB. Organic matter-rich layers are able to maintain oxygen depleted conditions due to capability of decaying organic matter to provide electrons for reactions of reduction. The presence of Fe^{2+} -bearing minerals, such as pyrite, vivianite and smectite in the La Playa sediments, as well as the low redox potential (around -230 mV, Table 5) of these sediments suggest that mineral transformation processes occurred in a reduced environment. In saline environments, such as that of La Playa dam (mean E.C. $2625 \mu S/cm$, Table 5), following the availability of easily degradable organic matter, microorganisms most likely can create unevenly microenvironments with reduced metals and aqueous sulfides, in which some processes lead to the precipitation of insoluble, heavy metal-bearing minerals.

Zinc sulfide mineral formation can play an important role for metal containment in wetlands (e.g., [41–43]). Zn sulfide is one of the most studied metal sulfides. Nanocrystalline spheroidal aggregates (up to $5 \mu m$) made of both ZnS polymorphs (sphalerite and wurtzite) have been described in low-temperature, near-surface environments [14,18].

The striking morphological and dimensional features of spherical and oval-shaped ZnS nanoparticle aggregates suggest bacterially induced precipitation of ZnS in the organic matter-rich sediments of La Playa sediments. Some studies have shown that ZnS grain crystallinity can be improved by the presence of *Desulfovibrio desulfuricans* producing biogenic crystals (sized 4–12 nm) of sphalerite and wurtzite [44]. In a Pb-Zn mine in Tennyson, Wisconsin (USA), the predominance of nanocrystals of sphalerite over those of wurtzite was revealed based on TEM data [43]. However, the small size of the nanoparticles from La Playa sediments made it difficult to obtain electron diffraction patterns and did not allow to distinguish the type of ZnS polymorph that form the observed cell-shaped aggregates.

SEM images showing the concentration of ZnS nanoparticles on the surface of the cell-shaped aggregates forming thin encrustations in the UCRB sediments (Figure 4a,b,e,h) suggest that precipitation of ZnS was associated to the activity of cell surfaces. SEM and HRTEM images of these sediments also revealed ZnS nanoparticles apparently not associated with cell-like morphologies (Figure 4b,c) suggesting that extracellular substances can also be involved in the nucleation of ZnS nanoparticles in the UCRB sediments. Therefore, the SEM and HRTEM data from this study suggest that sulfate-reducing bacteria cells facilitated decisively the uptake of Zn particles from UCRB sediments through sulfide minerals formation. Some experimental studies [45,46] have confirmed the ability of microbial cells to take up metals (Fe) that concentrate in crusts on the surface of microorganisms as sulfide minerals. Microscopy analyses [46] revealed that iron sulfide minerals produced in the presence of sulphate reducing microorganisms exhibit cell morphology with crusts, suggesting that the cell surface of live and dead sulphate-reducing microorganisms, and the extracellular polymers produced by live cells, provide templates for the nucleation of sulfide minerals and favor mineral growth. In this process, the nucleation of nanoparticles that take up pollutant metals can be favored by the effect of organic substances (extracellular polymeric substances, biofilms) that decrease free energy and act as ligands [18,41,47–49]. Particle attachment can produce larger nanocrystals and aggregates that can coarse to produce micrometric crusts [50]. Multiple stages of this process can promote botryoidal

habit. Becker et al. [51] suggested that the remobilization of heavy metals from reduced sediments is hampered by the predominance of sulfidic bonding. Microbially driven frambooidal pyrite formation can limit the mobility of metals from water and sediments and the abundance of plants can favor the incorporation of Zn within the roots [52]. Zn adsorption onto clay minerals cannot be discarded as an additional potential retention mechanism in the sediments [53–55].

Our results suggest that potentially toxic Zn, provided by different anthropogenic activities (wastewaters, agricultural and smelting activities), was concentrated in organic matter-rich sediments through precipitation of sulfides. The activity of sulfate-reducing microorganism controlled the formation of micron-scale cell-shaped aggregates made of ZnS nanocrystals.

6. Conclusions

Spatial distribution of Zn and other heavy metals in the sediments of the UCRB revealed that high concentrations of these metals are located in the slow flowing reaches associated to the clay minerals and organic matter-rich sediments from La Playa dam. Electron microscope evidence of Fe-Zn metallic particles in these sediments suggest that part of the supply of Zn into the UCRB was associated to the atmospheric deposit of particles from the activity of a local smelter located downstream the La Playa dam. Good correlations among organic matter, P₂O₅ and heavy metals contents suggest that the origin of Zn and other heavy metals can be, partially at least, in the same source as organic matter (wastewater discharges) and the agricultural activities upstream the La Playa dam (application of fertilizers, pesticides and fungicides).

Electron microscope evidence has also shown that the supply of Zn into the UCRB has been partially immobilized by biogenic metal sulfide crystallization in microsites of clay minerals and organic matter-rich sediments. Electron microscope images revealed dispersed ZnS nanoparticles and nanoparticles forming encrusted microbial shapes suggesting that sulfate-reducing microorganisms play essential role in the precipitation of Zn sulfides. This study has shown HRTEM and SEM proofs of the micro-scale mechanisms involved in the precipitation of biogenic Zn sulfide in polluted sediments. Nanoparticle precipitation associated to microbial organic substances in layers rich in decaying organic matter was the main mechanism of sulfide crystallization.

Supplementary Materials: The following are available online at <http://www.mdpi.com/2075-163X/10/8/673/s1>, Table S1: Major element sediment compositions determined by XRF and content in total organic carbon (TOC) (in weight percent); Table S2: Trace element sediment compositions determined by ICP-MS (for Cr, Ni, Cu and Pb) and XRF (for Zn) (in mg/kg); Table S3: Trace element water compositions at the sampling sites determined ICP-MS (in µg/L); Table S4: Physicochemical properties of the UCRB waters. R.P.: Redox potential. E.C.: Electrical conductivity.

Author Contributions: C.P.Q. and G.R.C. conducted field observations and sampling. J.J.-M., R.J.-E., C.P.Q. and G.R.C. performed microscopic observations SEM and TEM (mineralogical, textural, and geochemical analyses) and interpreted the X-ray diffractograms and chemical data (XRF and TOC). All the authors discussed the analytical results and prepared the manuscript. All authors have read and agreed to the published version of the manuscript.

Funding: This work has been financed by the Spanish research project PGC2018-094573-B-I00 from the MCIU-AEI-FEDER, and research group RNM-325 of the Junta de Andalucía (Spain). Our gratitude is also extended to Asociación Universitaria Iberoamericana de Postgrados (AUIP) and the Universidad de Boyacá. Additional thanks to Colombian Research groups Gestión Ambiental COL0005468 and Gestión de Recursos Hídricos COL0005477.

Acknowledgments: Technical and human support provided by CICT of Universidad de Jaén (UJA, MINECO, Junta de Andalucía, FEDER) is especially recognized for helping and for being able to provide us analyses during the COVID-19 lockdown. We acknowledge the suggestions and comments from two anonymous reviewers and from the editor.

Conflicts of Interest: The authors declare no conflict of interest. The funders had no role in the design of the study; in the collection, analyses, or interpretation of data; in the writing of the manuscript, or in the decision to publish the results.

References

1. Dietrich, D.; Huling, J.; Krekeler, M.P.S. Metal pollution investigation of Goldman Park, Middletown Ohio: Evidence for steel and coal pollution in a high child use setting. *Sci. Total Environ.* **2018**, *618*, 1350–1362. [[CrossRef](#)]
2. Yun, S.W.; Baveye, P.C.; Kim, D.H.; Kang, D.H.; Lee, S.Y.; Kong, M.J.; Park, C.G.; Kim, H.D.; Son, J.; Yu, C. Analysis of metal(loid)s contamination and their continuous input in soils around a zinc smelter: Development of methodology and a case study in South Korea. *Environ. Poll.* **2018**, *238*, 140–149. [[CrossRef](#)]
3. Marrugo-Negrete, J.; Pinedo, J.; Díez, S. Assessment of heavy metal pollution, spatial distribution and origin in agricultural soils along the Sinú River Basin, Colombia. *Environ. Res.* **2017**, *154*, 380–388. [[CrossRef](#)]
4. Poot, A.; Gillissen, F.; Koelmans, A. Effects of Flow Regime and Flooding on Heavy Metal Availability in Sediment and Soil of Dynamic River System. *Environ. Poll.* **2007**, *148*, 779–787. [[CrossRef](#)]
5. Derkach, T.; Khomenko, V. Essential and Toxic Microelements in the Medicinal Remedy Hyperichi herba by Different Producers. *Res. J. Pharm. Technol.* **2018**, *11*, 466–474. [[CrossRef](#)]
6. Chen, H.; Teng, Y.; Lu, S.; Wang, Y.; Wang, J. Contamination features and health risk of soil heavy metals in China. *Sci. Total Environ.* **2015**, *512*, 143–153. [[CrossRef](#)] [[PubMed](#)]
7. Shen, F.; Liao, R.; Ali, A.; Mahar, A.; Guo, D.; Li, R.; Sun, X.; Awasthi, M.K.; Wang, Q.; Zhang, Z. Spatial distribution and risk assessment of heavy metals in soil near a Pb/Zn smelter in Feng County, China. *Ecotoxicol. Environ. Saf.* **2017**, *139*, 254–262. [[CrossRef](#)]
8. Kabata-Pendias, A.; Mukherjee, A.B. *Trace Elements from Soil to Human*; Springer: Berlin/Heidelberg, Germany, 2007.
9. Yang, B.; Ren, J.; Wang, M.; Luo, H.; Cao, Y. Concentrations and chemical fractions of Cu, Zn, Cd, and Pb at ten metallurgical sites in China. *Environ. Sci. Poll. Res.* **2019**, *26*, 3603–3611. [[CrossRef](#)] [[PubMed](#)]
10. Nolan, A.L.; McLaughlin, M.J.; Mason, S.D. Chemical speciation of Zn, Cd, Cu, and Pb in pore waters of agricultural and contaminated soils using Donnan dialysis. *Environ. Sci. Technol.* **2003**, *37*, 90–98. [[CrossRef](#)]
11. Yang, Y.; Nan, Z.; Zhao, Z.; Wang, S.; Wang, Z.; Wang, X. Chemical fractionations and bioavailability of cadmium and zinc to cole (*Brassica campestris* L.) grown in the multi-metals contaminated oasis soil, northwest of China. *J. Environ. Sci. China* **2011**, *23*, 275–281. [[CrossRef](#)]
12. Foster, R.L.; Lott, P.F. X-ray diffractometry examination of air filters for compounds emitted by lead smelting operations. *Environ. Sci. Technol.* **1980**, *14*, 1240–1244. [[CrossRef](#)]
13. Han, F.X.; Banin, A.; Triplett, G.B. Redistribution of heavy metals in arid-zone soils under a wetting-drying soil moisture regime. *Soil Sci.* **2001**, *166*, 18–28. [[CrossRef](#)]
14. Castillo, J.; Pérez-López, R.; Caraballo, M.A.; Nieto, J.M.; Martins, M.; Costa, M.C.; Olías, M.; Cerón, J.C.; Tucoulou, R. Biologically-induced precipitation of sphalerite-wurtzite nanoparticles by sulfate-reducing bacteria: Implications for acid mine drainage treatment. *Sci. Total Environ.* **2012**, *423*, 176–184. [[CrossRef](#)] [[PubMed](#)]
15. Labrenz, M.; Druschel, G.; Thomsen-Ebert, T.; Gilbert, B.; Welch, S.; Kemner, K.; Logan, G.; Summons, R.; Gilbert, P.; Bond, P.; et al. Formation of Sphalerite (ZnS) Deposits in Natural Biofilms of Sulfate-Reducing Bacteria. *Science* **2001**, *290*, 1744–1747. [[CrossRef](#)] [[PubMed](#)]
16. Kosolapov, D.B.; Kuschk, P.; Vainshtein, M.B.; Vatsourina, A.V.; Wiessner, A.; Kästner, M.; Müller, R.A. Microbial processes of heavy metal removal from carbon-deficient effluents in constructed wetlands. *Eng. Life Sci.* **2004**, *4*, 403–411. [[CrossRef](#)]
17. Gadd, G.M.; White, C. Microbial treatment of metal pollution—A working biotechnology. *Trends Biotechnol.* **1993**, *11*, 353–359. [[CrossRef](#)]
18. Moreau, J.W.; Webb, R.I.; Banfield, J.F. Ultrastructure, aggregation state, and crystal growth of biogenic nanocrystalline sphalerite and wurtzite. *Am. Mineral.* **2004**, *89*, 950–960. [[CrossRef](#)]
19. Rodríguez-Zambrano, A.; Aranguren-Riaño, N. Comunidad planctónica de un embalse con alta tensión ambiental: La Playa, cuenca alta del río Chicamocha (Tuta, Boyacá), Colombia. *Biota Colomb.* **2014**, *15*, 95–110.
20. Silva-Rodríguez, J.D. Diseño de una red de logística inversa: Caso de estudio Usochicamocha—Boyacá. *Ing. Cienc.* **2017**, *13*, 91–113. [[CrossRef](#)]

21. Parra, L.; Sánchez, D. *Análisis de la Valorización de Escorias Negras Como Material Agregado Para Concreto en el Marco de la Gestión Ambiental de la Siderúrgica Diaco municipio de Tuta Boyacá*; Universidad de la Salle: Bogotá, Colombia, 2010.
22. Corpoboyacá—*Plan de ordenamiento del Recurso Hídrico de la Cuenca Alta y Media del Río Chicamocha*; Corpoboyacá: Tunja, Colombia, 2015.
23. Rodríguez, A.; Solano, O. Mapa Geológico del Departamento de Boyacá. In *Instituto de Investigaciones en Geociencias, Minería y Química—Ingeominas*; Ministerio de Minas y Energía de Colombia: Bogotá, Colombia, 2000.
24. Corpoboyacá—*Plan de Ordenación y Manejo Ambiental de la Cuenca Alta del Río Chicamocha*; Corpoboyacá—Corporación Autónoma Regional de Boyacá, Universidad Nacional de Colombia: Tunja, Boyacá, Colombia, 2006.
25. Márquez, G.; Guillot, G. *Ecología y efecto Ambiental de Embalses—Aproximación a Casos Colombianos*; Universidad Nacional de Colombia: Bogotá, Colombia, 2001; Volume 218.
26. Gazulla, M.F.; Vicente, S.; Orduña, M.; Ventura, M.J. Chemical analysis of very small-sized samples by wavelength-dispersive X-ray fluorescence. *X-Ray Spectrom.* **2012**, *41*, 176–185. [[CrossRef](#)]
27. Quevedo, C.P.; Jiménez-Millán, J.; Cifuentes, G.R.; Jiménez-Espinosa, R. Clay mineral transformations in anthropic organic matter-rich sediments under saline water environment. Effect on the detrital mineral assemblages in the upper Chicamocha river basin, Colombia. *Appl. Clay Sci.* **2020**, *196*, 105576. [[CrossRef](#)]
28. Azam, H.M.; Finneran, K.T. Fe(III) reductionmediated phosphate removal as vivianite ($\text{Fe}_3(\text{PO}_4)_2 \cdot 8\text{H}_2\text{O}$) in septic system wastewater. *Chemosphere* **2014**, *97*, 1–9. [[CrossRef](#)]
29. Kabata-Pendias, A. *Trace Elements in Soils and Plants*, 4th ed.; CRC Press: Boca Ratón, FL, USA, 2011.
30. Pérez-Sirvent, C.; Martínez-Sánchez, M.J.; García-Lorenzo, M.L.; Molina, J.; Tudela, M.L. Geochemical background levels of zinc, cadmium and mercury in anthropically influenced soils located in a semi-arid zone (SE, Spain). *Geoderma* **2009**, *148*, 307–317. [[CrossRef](#)]
31. De Almeida Júnior, A.B.; do Nascimento, C.W.A.; Biondi, C.M.; de Souza, A.P.; Barros, F.M.; do Rêgo Barros, F.M. Background and reference values of metals in soils from Paraíba state, Brazil. *Rev. Bras. Cienc. Sol.* **2016**, *40*, 1–13. [[CrossRef](#)]
32. Rueda-Saá, G.; Rodríguez-Victoria, J.A.; Madriñan-Molina, R. Methods for establishing baseline values for heavy metals in agricultural soils: Prospects for Colombia. *AcAg* **2011**, *60*, 203–218.
33. Martinez-Mera, E.; Torregroza, A.; Crissien-Borrero, C.J.; Marrugo, J.; González-Márquez, L. Evaluation of contaminants in agricultural soils in an Irrigation District in Colombia. *Heliyon* **2019**, *5*, e02217-10.
34. Gawlik, M.; Bidoglio, G. Background values in European soils and sewage sludges. Results of a JRC-coordinated study on background values. *Conclus. Comments Recomm.* **2006**, 22265.
35. Manceau, A.; Lanson, B.; Schlegel, M.L.; Harge, J.C.; Musso, M.; Eybert-Berard, L.; Hazemann, J.L.; Chateigner, D.; Lamble, G.M. Quantitative Zn speciation in smelter-contaminated soils by EXAFS spectroscopy. *Am. J. Sci.* **2000**, *300*, 289–343. [[CrossRef](#)]
36. Li, Z.; Feng, X.; Li, G.; Bi, X.; Sun, G.; Zhu, J.; Qin, H.; Wang, J. Mercury and other metal and metalloid soil contamination near a Pb/Zn smelter in east Hunan province, China. *Appl. Geochem.* **2011**, *26*, 160–166. [[CrossRef](#)]
37. Sajn, R.; Aliu, M.; Stafilov, T.; Alijagic, J. Heavy metal contamination of topsoil around a lead and zinc smelter in Kosovska Mitrovica/Mitrovice, Kosovo/Kosove. *J. Geochem. Explor.* **2013**, *134*, 1e16.
38. Ghayoraneh, M.; Qishlaqi, A. Concentration, distribution and speciation of toxic metals in soils along a transect around a Zn/Pb smelter in the northwest of Iran. *J. Geochem. Explor.* **2017**, *180*, 1–14. [[CrossRef](#)]
39. Li, P.; Lin, C.; Cheng, H.; Duan, X.; Lei, K. Contamination and health risks of soil heavy metals around a lead/zinc smelter in southwestern China. *Ecotoxicol. Environ. Saf.* **2015**, *113*, 391–399. [[CrossRef](#)] [[PubMed](#)]
40. Silva, S.M.; Correa, F.J. Análisis de la contaminación del suelo: Revisión de la normativa y posibilidades de regulación económica. *Semest. Econ.* **2009**, *12*, 13–34.
41. Yoon, S.; Yañez, C.; Bruns, M.A.; Martinez-Villegas, N.; Martinez, C.E. Natural zinc enrichment in peatlands: Biogeochemistry of ZnS formation. *Geochim. Cosmochim. Acta* **2012**, *84*, 165–176. [[CrossRef](#)]
42. Cabała, J.; Smiejka-Król, B.; Jabłonska, M.; Chrost, L. Mineral components in a peat deposit: Looking for signs of early mining and smelting activities in Silesia-Cracow region (Southern Poland). *Environ. Earth Sci.* **2013**, *69*, 2559–2568. [[CrossRef](#)]

43. Smieja-Krół, B.; Janeczek, J.; Bauerek, A.; Thorseth, I.H. The role of authigenic sulfides in immobilization of potentially toxic metals in the Bagno Bory wetland, southern Poland. *Environ. Sci. Poll. Res.* **2015**, *22*, 15495–15505. [[CrossRef](#)]
44. Xu, J.; Murayama, M.; Roco, C.M.; Veeramani, H.; Michel, F.M.; Rimstidt, J.D.; Winkler, C.; Hochella, M.F., Jr. Highly-defective nanocrystals of ZnS formed via dissimilatory bacterial sulfate reduction: A comparative study with their abiogenic analogues. *Geochim. Cosmochim. Acta* **2016**, *180*, 1–14. [[CrossRef](#)]
45. Ferris, F.G.; Fyfe, W.S.; Beveridge, T.J. Bacteria as nucleation sites for authigenic minerals in a metal-contaminated lake sediment. *Chem. Geol.* **1987**, *63*, 225–232. [[CrossRef](#)]
46. Picard, A.; Gartman, A.; Clarke, D.R.; Girguis, P.R. Sulfate-reducing bacteria influence the nucleation and growth of mackinawite and greigite. *Geochim. Cosmochim. Acta* **2018**, *220*, 367–384. [[CrossRef](#)]
47. Cho, K.S.; Talapin, D.V.; Gaschler, W.; Murray, C.B. Designing PbSe nanowires and nanorings through oriented attachment of nanoparticles. *J. Am. Chem. Soc.* **2005**, *127*, 7140–7147. [[CrossRef](#)]
48. Dey, A.; Bomans, P.H.; Müller, F.A.; Will, J.; Frederik, P.M.; de With, G.; Sommerdijk, N.A. The role of prenucleation clusters in surface-induced calcium phosphate crystallization. *Nat. Mater.* **2010**, *9*, 1010–1014. [[CrossRef](#)] [[PubMed](#)]
49. De Yoreo, J.J.; Gilbert, P.U.P.A.; Sommerdijk, N.A.J.M.; Penn, R.L.; Whitelam, S.; Joester, D.; Zhang, H.; Rimer, J.D.; Navrotsky, A.; Banfield, J.F.; et al. Crystallization by particle attachment in synthetic, biogenic, and geologic environments. *Science* **2015**, *349*, 6247. [[CrossRef](#)] [[PubMed](#)]
50. Falk, N.; Chaganti, S.R.; Weisener, C.G. Evaluating the microbial community and gene regulation involved in crystallization kinetics of ZnS formation in reduced environments. *Geochim. Cosmochim. Acta* **2018**, *220*, 201–216. [[CrossRef](#)]
51. Becker, A.; Klöck, W.; Friese, K.; Schreck, P.; Treutler, H.C.; Spettel, B.; Duff, M. Lake Süßer See as a natural sink for heavy metals from copper mining. *J. Geochem. Explor.* **2001**, *74*, 205–217. [[CrossRef](#)]
52. Giudici, G.; Pusceddu, C.; Medas, D.; Meneghini, C.; Gianoncelli, A.; Rimondi, V.; Podda, F.; Cidu, R.; Lattanzi, P.; Wanty, R.; et al. The role of natural biogeochemical barriers in limiting metal loading to a stream affected by mine drainage. *Appl. Geochem.* **2016**, *76*. [[CrossRef](#)]
53. Kaya, A.; Oren, A.H. Adsorption of zinc from aqueous solutions to bentonite. *J. Hazard. Mater.* **2005**, *125*, 183–189. [[CrossRef](#)]
54. Malamis, S.; Katsou, E. A review on zinc and nickel adsorption on natural and modified zeolite, bentonite and vermiculite: Examination of process parameters, kinetics and isotherms. *J. Hazard. Mater.* **2013**, *252*, 428–461. [[CrossRef](#)]
55. Lahori, A.H.; Vu, N.H.; Du, J.; Quang, T.D.; Saif, U.R.; Zobia, N.; Munee, A.; Zengqiang, Z. Stabilization of toxic metals in three contaminated soils by residual impact of lime integrated with biochar and clays. *J. Soils Sedim.* **2020**, *20*, 734–744. [[CrossRef](#)]



© 2020 by the authors. Licensee MDPI, Basel, Switzerland. This article is an open access article distributed under the terms and conditions of the Creative Commons Attribution (CC BY) license (<http://creativecommons.org/licenses/by/4.0/>).